Korean J. Chem. Eng., 37(12), 2248-2261 (2020)
DOI: 10.1007/s11814-020-0653-8

pISSN: 0256-1115
eISSN: 1975-7220

Antifouling properties of poly(vinylidene fluoride)-incorporated cellulose acetate composite ultrafiltration membranes

Manikandan Gomathy Nainar, Kalidass Jayaraman, Helen Kalavathy Meyyappan†, and Lima Rose Miranda

Department of Chemical Engineering, A C Tech, Anna University, Chennai-600 025, India
(*Received 1 February 2020 • Revised 2 June 2020 • Accepted 3 August 2020*)

Abstract−Poly(vinylidene fluoride) (PVDF) was incorporated in Cellulose acetate (CA) to prepare polymeric blend membrane to enhance the antifouling properties and rejection. Blend membranes consist of different concentrations (0, 2.5 and 5.0 wt%) of polyvinylpyrrolidone (PVP), which was the hydrophilic polymer additive and pore forming agent. The existence of membrane functional groups was analyzed by ATR-FTIR spectroscopy. AFM and SEM were conducted to explain the surface morphology of the synthesized blend membranes. Membrane properties were examined by contact angle, porosity and equilibrium water content (EWC). The membrane's thermal and mechanical properties were determined by performing TGA and tensile test. Membrane performance was assessed by pure water flux (PWF), rejection, antifouling properties using bovine serum albumin (BSA) and Sodium alginate (SA) solution. In this study, CPA-2 membrane showed high PWF of 269.82 L m^{-2} h^{-1}, flux recovery ratio (FRR) against BSA and SA was 94% and 92%, respectively. Rejection of BSA and SA was found to be 83% and 86%, respectively. From the results, it was significant that the hydrophilic additive PVP blended membrane ameliorated and showed better results in surface roughness, hydrophilicity, thermal and mechanical stability. Hence, CPA-2 membrane would exhibit less susceptibility to fouling with enhanced PWF, permeability and selectivity.

Keywords: Cellulose Acetate, Poly(Vinylidene Fluoride), Polymer Blend, Bovine Serum Albumin, Sodium Alginate

INTRODUCTION

Nowadays, the most common problem is insufficient fresh water on the globe, and it is getting worse year-by-year because of speed in population growth, high industrialization, drastic climate change and poor wastewater management systems. Current research work is focused on producing hygienic potable water and every researcher believes that the water and sanitation crisis can be cleared within our lifetime. Though there are many conventional techniques for the removal and recovery of pollutants or valuable products, membrane separation process has attracted many researchers due to its ease of operation and distinctive separation; in other words, selective transport which results in effective separation when compared to different techniques [1]. Furthermore for membrane separations, no chemical additives are required and they are performed in ambient conditions, which involve very less energy consumption [2]. Many literatures concentrate on removing harmful chemicals, natural organic matter (NOM), particulates (e.g., soot and silt), viruses and bacteria [3]. This work concentrates on both rejection and membrane fouling studies.

Membrane synthesis plays an indispensable role in the separation of particular components and the preparation of these membranes becomes more attractive after the imposition of phase inversion technique [2]. The membrane process shows advantageous properties, such as selective transport, quality product and high efficiency, over other conventional separation processes. Despite the many advantages, their application is limited because of membrane fouling caused by organic components, which will increase energy consumption and replacement cost [3]. Membrane fouling has two types, reversible and irreversible fouling, resolved by performing physical cleaning for the former and chemical cleaning for the latter [4].

In membrane separation, the rejection of NOM is more difficult because NOM is an intricate heterogeneous composition of humic substances, polysaccharide, carbohydrates, and proteins [4]. NOM is considered as the main defective foulant that causes irreversible membrane fouling [5]. It has two components: hydrophobic and hydrophilic. Hydrophobic components consist of humic substances and hydrophilic components are polysaccharide and protein substances [6]. These substances are the main cause for membrane fouling in micro-filtration and ultrafiltration processes. Because of the hydrophobic nature of the humic acid, it can be easily rejected by the membrane, which leads to relatively less flux decline [5,6]. On the other hand, polysaccharide being hydrophilic gets adsorbed over the membrane surface and due to which there is a decline in flux. Consequently, the hydrophilic components had more severe fouling potential than the hydrophobic component [7].

In recent times, research carried out on sewage treatment technology has reported the presence of sodium alginate in large quantity, which is synthesized from organic substance present in wastewater [8]. Sodium alginate ($(C_6H_8O_6Na)_n$), being a complex natural polysaccharide, cannot be separated using conventional treatment methods and therefore membrane separation has found its place in the separation and retrieval of alginate [8]. The recovered

†To whom correspondence should be addressed.
E-mail: helenkalavathy@gmail.com

alginate has many applications in various industries such as food, textile, paper, printing, and pharmaceutical [4,8]. Meanwhile, the alginate separation and recovery creates major fouling over the surface of membrane, which lessens the membrane life and water flux [9]. Therefore, to lower the fouling of membrane and to increase water flux, a hydrophilic group was implanted on the surface of the polymer because it usually favors the diffusion of water molecules through the membranes [10]. To implant hydrophilicity, there are several methods such as surface coating, UV-irradiation and grafting. These methods are very complex and require more hazardous chemicals as additive [11]. The most simple and effective technique is polymer blending, which is easier to synthesize a new material with enhanced basic transport properties of base polymer in the membrane. Different polymers, such as cellulose acetate, poly ether sulfone, PVC, polysulfone, poly (vinylidene fluoride), poly ether imide, and poly acrylo nitrile, are involved, which helps to improve the required characteristics for separation and at the same time retaini their individual characteristics [12].

In this study, the chosen base polymer is cellulose acetate, which has a special ability to perform concentration and separation in one step for ultrafiltration. Cellulose acetate has built-in characteristics such as tough biocompatibility, relatively easy availability, renewable raw material, economically cost effective and ecofriendly [2]. In membrane development, it is largely applicable due to its hydrophilicity; it results in good fouling resistance, high flux and good desalting nature. However, in CA membrane, the major drawback is the inadequacy of reactive functional unit over the polymer backbone to enhance the membrane separation efficiency [12]. Moreover, CA membrane is also not suitable for aggressive backwashing because it has low chemical and oxidation resistance and low mechanical stability [13,14]. These limitations restrict the utilization of cellulose acetate membrane for treatment of wastewater [11]. Hence, cellulose acetate membrane needs significant surface modification.

In the current work, cellulose acetate membranes were modified with poly (vinylidene fluoride), a semicrystalline polymer, which exhibits remarkable features like good thermal stability, chemical resistance, mechanical properties and restricted porosity. Also, its oxidant resistance makes the polymer an appropriate membrane material for processing wastewater [11,15]. This blending balances the hydrophilic and hydrophobic characteristics of the multicomponent polymer blends. Meanwhile, the use of PVDF is limited in the aqueous phase because of its hydrophobic nature, which clearly delineates the low flux rate and its anti-fouling characteristic in membranes [16]. Thus, the pore size distribution of the membrane is improved through addition of pore forming additive such as polyethylene glycol (PEG), polyvinyl pyrrolidone (PVP), polyethylene oxide (PEO), which resulted in the improvement of membrane performance studies [17]. The pore forming agent, PVP, used plays a key role in the formation of pores in asymmetric membranes. This also promotes hydrophilicity on the membrane surface with more pore size distribution and reduces the fouling property with increased flux rate.

Hence, an attempt has been made in preparing cellulose acetate/poly (vinylidene fluoride) blend membrane with pore forming additive PVP to study the rejection and antifouling properties of composite membranes against BSA and sodium alginate.

MATERIALS AND METHODS

1. Materials

Cellulose Acetate (CA) was used as a base polymer supplied from Loba Chemie Pvt. Ltd., India. Poly (vinyldiene fluoride) (PVDF) and polyvinylpyyrolidone (PVP) were acquired from Alfa Aesar, India. The solvents dimethylformamide (DMF) and sodium lauryl sulphate (SLS) were procured from Sisco Research Laboratories Pvt. Ltd., India. Bovine Serum Albumin was procured from CSIR Biochemical Centre, India and sodium Alginate (SA) was procured from Sigma Aldrich, India.

2. Preparation of CA/PVDF Membranes

CA/PVDF blend membranes were prepared in the presence of PVP as a pore forming agent, through non-solvent induced phase separation (NIPS) method. The dope solutions were dissolved in a preferred volume of DMF under constant stirring for 24 h at 60 °C to form a homogeneous mixture. The obtained mixture was degassed for another 24 h at the same temperature. The casting solution was cast over glass plate using a casting knife and then permitted to vaporize for 30 s at 18% relative humidity. Further, the glass plate was placed inside the precipitation bath containing water, where exchange of solvent and non solvent occurred to complete the phase separation process. After 24 h, the membranes were taken from the glass plate and then completely cleaned by using water to discard the excess footprints of DMF. Similarly, the pristine CA membrane and CA/PVDF blend membrane were prepared without additive. The synthesized membranes were used for further study. The solution composition of each membrane is shown in Table 1.

3. Characterization of Membrane

3-1. ATR-FTIR Analysis

The functional groups present in the composite membrane surface were investigated by FTIR - attenuated total reflectance (ATR) studies. The ATR-FTIR spectra were recorded using Spectrum RXI, Perkin Elmer spectrometer range from 4,000-400 cm^{-1}.

3-2. Membrane Surface Morphology

The prepared membranes were cut into dimensions of 1 cm× 1 cm to analyze the cross sectional morphology using scanning electron microscope (SEM-Hitachi S-300400N). The prepared membranes were fractured in liquid Nitrogen (N_2) for 1 minute.

3-3. Membrane Topography

The modification on the surface topography and roughness of the developed membranes were examined by atomic force micros-

Table 1. Chemical composition of casting solution for CA/PVDF membranes

Membrane	Polymer (18 wt%)		Additive (wt%)	Solvent (wt%)
	CA	PVDF	PVP	DMF
Pristine	100	0	0	82
CPA-0	85	15	0	82
CPA-1	85	15	2.5	79.5
CPA-2	85	15	5.0	77.5

copy (Par, XE-100). Roughness of the prepared membrane surface (1 cm×1 cm) was investigated by using tapping mode and the surfaces were imaged at the rate of 5 μm×5 μm scan size.

3-4. Viscosity Measurement

The rheological study of the dope solution was analyzed using Anton Paar rheometer. The viscosity of the solution was examined at 100 s^{-1} shear rate with a revolution of 20 rpm at 30 °C.

3-5. Porosity

The porosity of the membrane was determined by soaking the membranes in distilled water for 4 h at room temperature; the membranes were patted with the dry blotting paper to measure the wet weight (W_w). To measure the dry weight (W_d) of the membrane, the wet membranes were positioned in an oven for a whole day at 50 °C. From the two weights of the membrane, the surface porosity (ε) was estimated using the following equation [11,18,19]:

$$\varepsilon(\%)=\frac{W_w-W_d}{\rho A l}\times 100 \quad (1)$$

where, ε is the porosity of the membrane, W_w and W_d are the wet and dry weight of the membrane sample (g), ρ is density of pure water (g cm^{-3}), A is the area of the membrane (cm^2) and l is the thickness of the membrane (cm). The average values of five different samples of same composition were taken to measure the membrane porosity.

3-6. Mean Pore Size Measurements

The mean pore size of the membranes was examined by water filtration velocity method and the outcomes were evaluated at constant operating pressure (0.3 MPa). The mean pore radius was evaluated using Guerout-Elford-Ferry equation as follows [20,21]:

$$r_m=\sqrt{\frac{(2.9-1.75*\varepsilon)8\eta l Q}{\varepsilon A \Delta P}} \quad (2)$$

where ε is the porosity, η is the water viscosity ($8.9*10^{-4}$ Pa·s), l is the membrane thickness (m), Q is the volume of the permeate per unit time (m^3s^{-1}) and ΔP is the trans-membrane pressure (Pa).

3-7. Equilibrium Water Content (EWC)

Equilibrium water content (EWC) is the property to determine the water uptake in the membrane. The prepared membranes (1 cm ×1 cm) were placed inside the water for 24 h and wet weight was measured after dabbing with dried filter paper. Wet membranes were dried in an oven at 40 °C for 24 h and the membranes were weighed again to measure the dry weight. Then, EWC outcomes were evaluated subsequently by the following equation [22,23]:

$$EWC(\%)=\frac{\text{Wet weight } (W_w)-\text{Dry weight } (W_d)}{\text{Wet weight } (W_w)}\times 100 \quad (3)$$

The average values of EWC were measured by taking five different samples of same composition of the prepared membranes.

3-8. Water Contact Angle (WCA) Measurements

Water contact angle (OCA 15 EC, Data Physics, Germany) measurements were made to determine the hydrophilicity of the prepared membranes. The sessile drop method was used to measure the contact angle at ambient operating condition. The prepared membranes in the dimension of 3 cm×6 cm were washed completely with the water and the excess moisture content was removed from the membrane surface using filter paper. Then the membranes were kept on a glass plate to study the polar interactions between the membrane and water interfaces. Subsequently, the volume of 5 μL of water was slowly located on the membrane surface using a small needle without any air bubbles to measure the contact angle. To identify the accuracy of WCA, the average values of each membrane were taken at four different spots. From the contact angle measurements, the interactive forces among the solid and liquid surfaces were evaluated by work of adhesion using Young-Dupree equations [24-26]:

$$W_a=(1+\cos\theta)\Upsilon_{lv} \quad (4)$$

$$\Upsilon_{sl}=\Upsilon_{sv}-\Upsilon_{lv}\cos\theta \quad (5)$$

$$S_c=\Upsilon_{sv}-\Upsilon_{sl}-\Upsilon_{lv} \quad (6)$$

$$\cos\theta=-1+2\sqrt{\frac{\Upsilon_{sv}}{\Upsilon_{lv}}}e^{-\beta(\Upsilon_{lv}-\Upsilon_{sv})^2} \quad (7)$$

where, Υ_l, Υ_{sv} and Υ_{sl} are the interfacial free energies of liquid-vapor, solid-vapor and solid-liquid phases, respectively, β is the constant value of 0.0001024 mJm^{-2} and θ corresponds to the solid-liquid contact angle measurement.

3-9. Thermal and Mechanical Properties of the Membrane

The thermal behavior of the prepared membranes was analyzed using universal TGA Q50 V20.5 Build 30 analysis in nitrogen atmosphere and heated up to 800 °C at a heating rate of 5 °C/min.

The mechanical property of the fabricated membranes was investigated by tensile strength and defined by stress-strain curves using Instron 3369 analyzer having a stretching rate of 5 mm min^{-1} at room temperature. Each membrane sample was cut into 12 cm× 3 cm and excess water was removed before testing. The results were taken from the three average values of each membrane.

4. Permeation Studies

4-1. Ultrafiltration Test

Fig. 1 shows the batch type dead end ultrafiltration cell with an internal diameter of 6.5 cm with Teflon coated magnetic propel used to conduct the permeation and rejection studies of all the

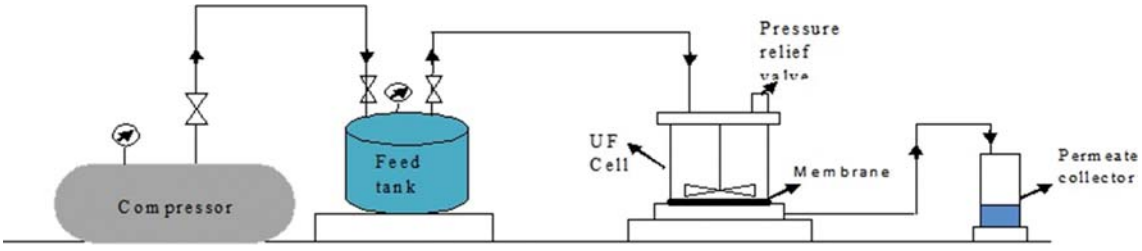

Fig. 1. Ultrafiltration experimental setup.

developed membranes. This cell has pressure control valve and gauge received from compressor to the feed chamber. The area of membrane that was effectively accessible for ultrafiltration was 33.17 cm^2 with a volumetric capacity of 200 mL and the solution in the cell was stirred at 245 rpm.

The water permeation performance studies of prepared membranes were determined using deionized water in above-mentioned ultrafiltration cell. Initially, membranes were compacted at 0.4 MPa TMP for an hour to remove any remaining solvent or unreacted polymer. Following compaction, membranes were subjected to a constant TMP (0.3 MPa) to evaluate pure water flux with time till it attained steady state conditions at room temperature. The PWF was measured by employing Eq. (8) [27]:

$$J_{v1}=\frac{Q}{A\cdot\Delta t} \tag{8}$$

where J_{v1}: PWF of fresh membrane (L m^{-2} h^{-1}), Q: volumetric flow rate of water permeated (L h^{-1}), A: effective surface area of the membrane (m^2) and Δt: time duration of permeate (h).

4-2. Antifouling Properties

For antifouling properties, three sets of experiments were conducted for each sample of synthesized membrane. The membrane properties--antifouling property and flux recovery ratio (FRR)--were determined by carrying out the following steps. First, the initial pure water flux was performed at 0.3 MPa TMP for 5 h. Then, the prepared BSA and Sodium alginate solutions at a concentration of 1 g/L were screened via membrane for every one hour and the protein permeate flux (J_p) and sodium alginate permeate flux (J_s) were noted. After BSA and SA filtration, the membrane was kept in SLS solution for 10 minutes and, finally, washed with double distilled water for 10 minutes and final pure water flux (J_{v2}) was evaluated.

Thereafter, the membrane antifouling performance studies were measured in terms of flux recovery ratio (FRR) using Eq. (9) [28]. Generally higher flux recovery ratio resembles better antifouling behavior of the membrane.

$$FRR(\%)=\left(\frac{J_{v2}}{J_{v1}}\right)\times 100 \tag{9}$$

Reversible and irreversible protein fouling (R_r and R_{ir}) were used to measure the flux loss using Eqs. (10) and (11) [28,29]:

$$R_r(\%)=\left(\frac{J_{v2}-J_p}{J_{v1}}\right)\times 100 \tag{10}$$

$$R_{ir}(\%)=\left(\frac{J_{v1}-J_{v2}}{J_{v1}}\right)\times 100 \tag{11}$$

The total fouling (R_t) of the membrane was calculated using Eq. (12).

$$R_t(\%)=\left(\frac{J_{v1}-J_p}{J_{v1}}\right)\times 100 \tag{12}$$

4-3. Bovine Serum Albumin (BSA) and Sodium Alginate (SA) Rejection Study

The prepared membrane rejection behavior was determined with 1 g/L of BSA and SA solution in the feed reservoir. The membrane rejection efficiency was examined by filtration method. The feed and permeate concentration of BSA and SA solutions were evaluated by TOC analyzer (Shimadzu, TOC-VCPH). The rejection efficiency of BSA and SA of the prepared membrane was examined by Eq. (13) [29]:

$$R(\%)=\left(1-\frac{C_p}{C_f}\right)\times 100 \tag{13}$$

where C_f is feed concentration (g/L) and C_p is permeate concentration (g/L).

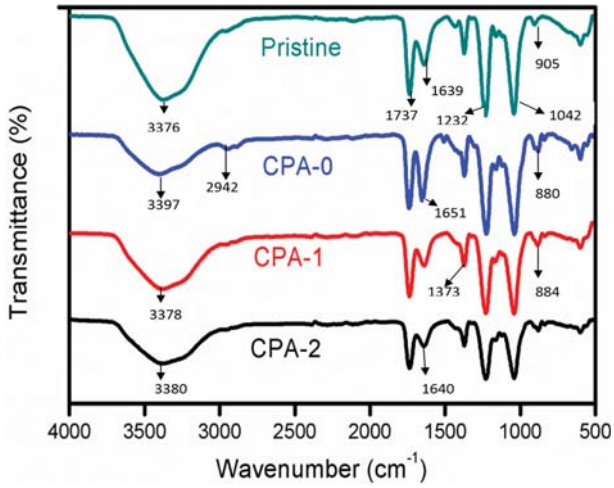

Fig. 2. ATR-FTIR results of prepared membranes.

RESULTS AND DISCUSSION

1. ATR-FTIR Analysis

The obtained ATR-FTIR spectra of the pristine CA and CA/PVDF blend membranes of different compositions of PVP (CPA-0, CPA-1 and CPA-2) presented in Fig. 2 exhibit the existence of functional groups. The spectrum of pristine CA membrane IR bands at 3,376 cm^{-1} stretching represents a very broad peak of -OH group. The weak stretching peak at 2,103 cm^{-1} points to C≡C group and the sharp peak at 1,737 cm^{-1} shows strong stretching frequency of -C=O group of CA [30]. The medium stretching spectra at 1,639 cm^{-1} signifies C=C group of alkenes. The existence of variable bands at 1,432 and 1,373 cm^{-1} with scissoring and bending indicates C-H group of alkanes. The prominent IR absorption bands at 1,232 to 1,042 cm^{-1} are related to C-C (O)-C stretch of acetate ester of CA. The specific peak at around 905 cm^{-1} represents the out-of-plane curving of C-H vibration [31]. In the CPA-0 membrane, the spectrum shows some switchover in the frequencies (stretch) of functional group with shifting wavenumbers compared to pristine membrane. The -OH group of pristine membrane at 3,376 cm^{-1} was shifted to 3,397 cm^{-1} in CPA-0 membrane. The C-H group is present at 2,942 cm^{-1} with asymmetric and symmetric stretching vibrations of alkyl groups [-$(CH)_n$-]. The sharp absorption peak at 1,739 cm^{-1} corresponding to the strong stretching frequency of -C=O of CA and medium stretching at 1,651 cm^{-1} relating to C=C group of alkenes and the weak band at 1,372 cm^{-1} suggested C-H in-plane bending or scissoring alkane group similar to that of pristine membrane. Consequently, the IR absorption band shows the

presence of γ-phase of PVDF at 1,225 cm^{-1}. The spectrum at 1,163 and 1,038 cm^{-1} is associated with the symmetrical stretching of -CF_2 group. The spectrum band at 880 cm^{-1} represents the combined mode of CH_2 and CF_2 asymmetric stretching in β and γ-phase of PVDF [32]. The spectrum at 760 cm^{-1} is associated with in-plane bending or rocking vibration in α-phase of PVDF. Further, the incorporated PVP of CPA-1 and CPA-2 membranes showed the presence of similar and shifted spectra bands as in Fig. 2. In comparison with CPA-0 membrane, the CPA-1 and CPA-2 membrane spectra bands of -OH group got shifted to 3,378 and 3,380 cm^{-1}, alkene group of C=O was shifted to 1,639 and 1,640 cm^{-1}, respectively, and other spectra bands such as 1,737, 1,373, 1,229, 1,040 and 884 cm^{-1} are similar to CPA-0 membrane. On comparing the membranes with and without additive, FTIR spectra bands were shifted but the functional groups were the same in the blend membranes. This clearly shows that the blend membrane has good compatibility and better homogeneity/miscibility of dope solution. Subsequently, the results of FTIR prove that there is no interaction between PVP and DMF in CA/PVDF blend; because of phase inversion process, DMF and water exchange occurs and the pore forming additive PVP has been seeped out of the membrane matrix and formed pores on the membrane surface.

2. Membrane Surface Morphology

The surface and cross sectional morphology of the developed membranes was evaluated through scanning electron microscopy and depicted in Fig. 3. The SEM images clearly show the formation of the asymmetric structure along with the thin skin layer supported by thicker sponge- or finger-like substructure. The asymmetric membrane formation is due to the high exchange rate of influx of water molecules in comparison to the solvent outflow, and this is mainly because of the high diffusion coefficient of water molecules. Also, since the solvent has strong affinity towards the non-solvent, they intermix with each other immediately, as a result of which a thin skin layer and thicker porous substructure is formed, which contributes to the mechanical strength of the developed membrane. Increased resistance is offered to the movement of material by the skin layer at the top, and thicker porous sublayer offers low resistance to material transport.

Fig. 3(a) shows the cross sectional morphology of the pristine cellulose acetate membrane without PVDF and PVP. The pristine membrane exhibits macrovoids and the pores are not completely unlocked. Before film formation, the attraction of CA towards water remains for an extended period of time, allowing exchange between solvent and non-solvent. Therefore, the open transition sublayer is hard to form in pristine membrane and this is due to the slow diffusion process of water molecules, which is due to the viscosity of dope solution and the interface between water and polymer in the membrane.

The SEM image of CPA-0 membrane without additive is shown in Fig. 3(b). The addition of PVDF to CA leads to the disappearance of some macrovoids, resulting in the formation of narrow pore structure. The formation of these pores is due to the higher blend solution viscosity that lowers the diffusional exchange rate between solvent and non-solvent and this contributes to delayed demixing of the membrane. Hence, the development of the skin layer is reduced and the emergence of narrow pores is improved in the sublayer, which is clearly seen from Fig. 3(b). However, some macrovoids appear and this could be due to the absence of additive.

Fig. 3(c) and 3(d) shows the morphology of CA/PVDF blend membrane with PVP additive of 2.5% and 5%, respectively. The impact on addition of PVP was clearly perceived from the SEM images. PVP, on addition to the blend solution, has double effect on the membrane structure. When PVP was added to CA/PVDF blend, it created immediate demixing and thus led to the develop-

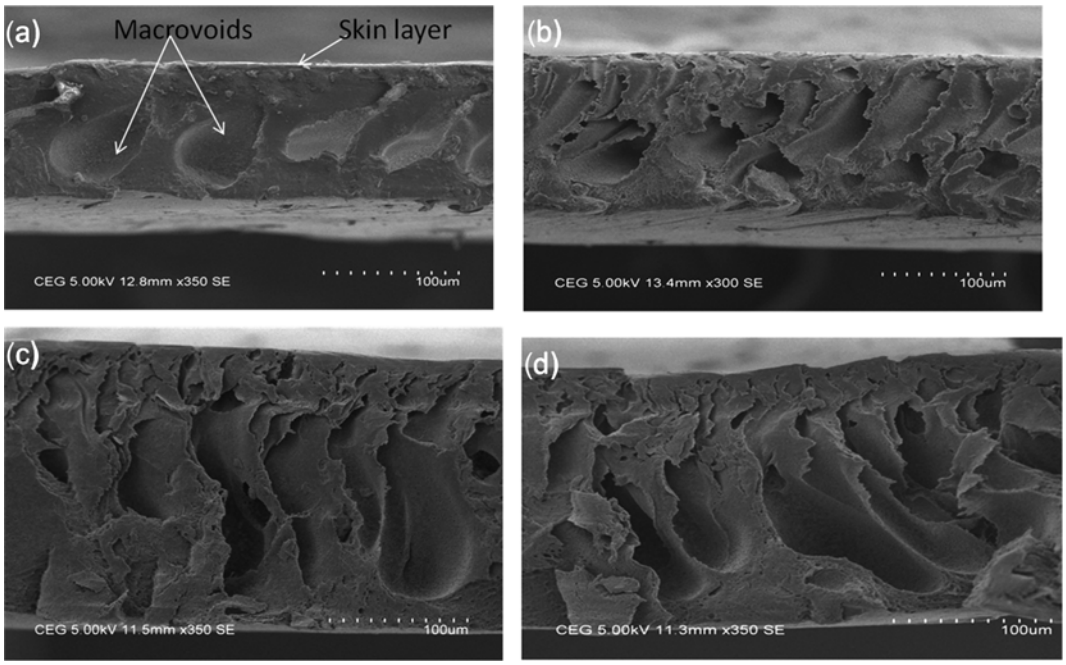

Fig. 3. Cross-sectional SEM images of the (a) Pristine (b) CPA-0 (c) CPA-1 and (d) CPA-2 membranes.

ment of macrovoids in the sublayer of membrane. At the same time, the addition of PVP increases the dope solution viscosity which slows the rate of exchange between solvent and non solvent in the process of membrane formation. Hence, this resulted in delayed demixing, thereby suppressing the macrovoids and forming finger-like and denser structure over the membrane surface. As the wt% of PVP increased from 2.5% to 5%, the size of pores on the membrane surface and pore size distribution also increased. Also, the pores that were formed were narrow, uniform, well developed and extended till the bottom of the membrane surface with tortuous path.

Therefore, it is evident that CPA-2 membrane showed better pore formation when compared to other membranes.

3. Membrane Topography

To analyze the effect of the PVP on CA/PVDF blend membrane morphology and surface roughness, Atomic force microscopy (AFM) was conducted. Fig. 4 displays the 2D and 3D of AFM images of Pristine, CPA-0, CPA-1 and CPA-2. From the images, it is evident that the introduction of PVP had a strong impact on membrane surface morphology. The values of mean roughness profile (R_a), root

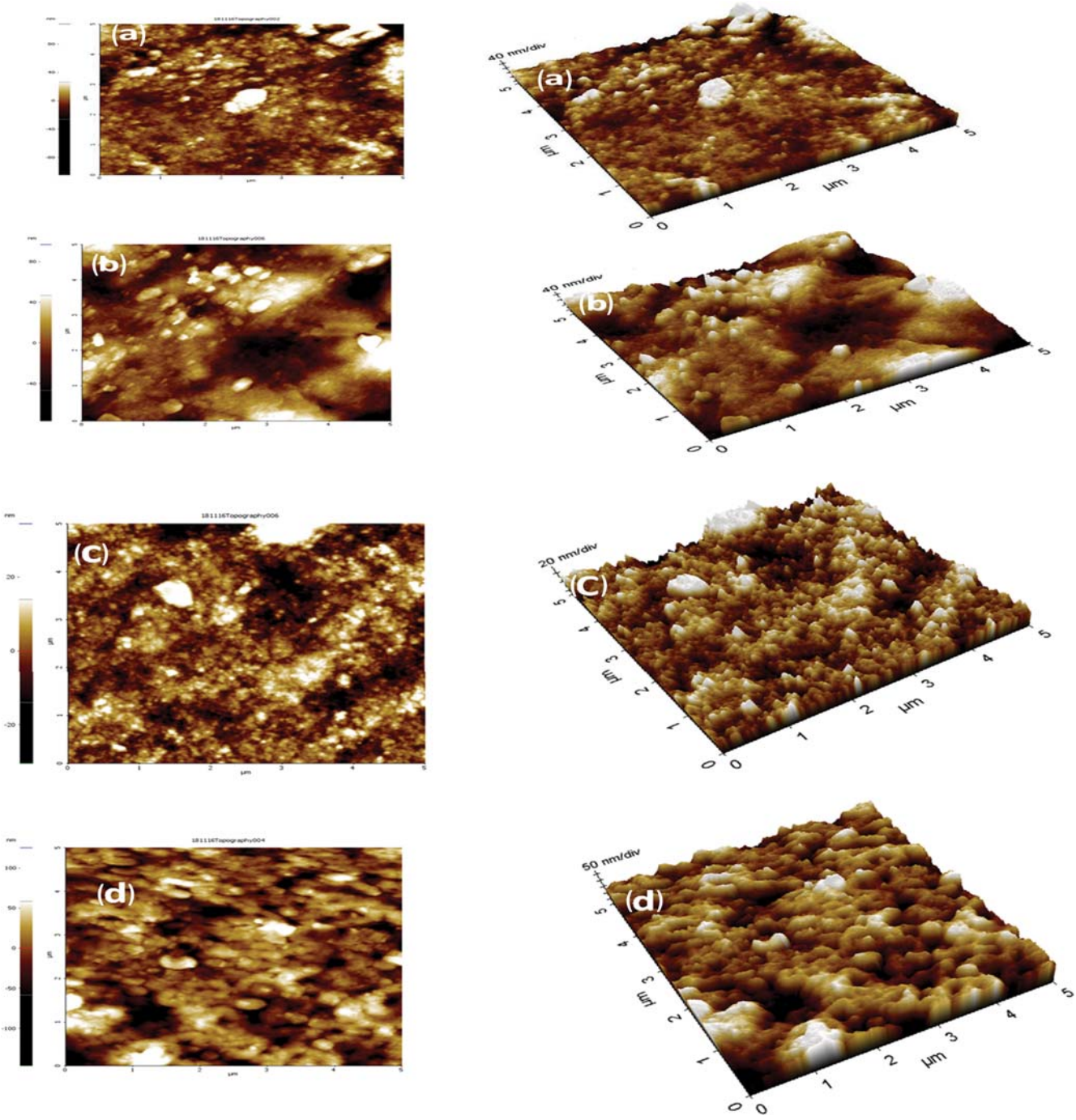

Fig. 4. 2D and 3D AFM Topography images of (a) Pristine, (b) CPA-0, (c) CPA-1 and (d) CPA-2.

Table 2. Roughness parameters of the membrane

Membrane	Roughness parameters			
	R_a (nm)	R_q (nm)	R_{max} (nm)	R_T (nm)
Pristine	9.271	13.384	200.919	212.983
CPA-0	18.754	25.842	210.875	233.827
CPA-1	20.572	27.351	238.126	254.243
CPA-2	22.621	29.723	266.052	271.872

mean square deviation roughness (R_q), maximum height of the roughness profile (R_{max}) and total height of the roughness profile (R_T) are displayed in Table 2. R_a is defined as deviation in height over the surface, R_q represents the standard deviation of surface heights, R_{max} is height of the highest peak above the mean line of the surface and R_T represents the total mean of the maxima profile of both peak height and valley depth of the surface. The pristine CA membrane showed the R_a, R_q, R_{max} and R_T as 9.271 nm, 13.384 nm, 200.919 nm and 212.983 nm, respectively, whose values are very much lower when compared to other membranes. This is because of the viscosity of dope solution and there is a restriction in the formation of a valley because of its high crystalline structure [1]. Thus, the pristine membrane showed a decrease in surface roughness. In CPA-0 membrane, the surface roughness R_a (18.754) and R_q (25.842) values were increased when compared to pristine membrane. This is because of the fact that on addition of PVDF more nodules (peaks) and pores (valleys) appeared over the membrane surface giving rise to increased surface roughness. Considering CA/PVDF/PVP blend membrane, as the concentration of the PVP increases, there is a slight increase in the R_a and R_q values: 20.572 and 27.351 for CPA-1 and 22.621 and 29.723 for CPA-2, respectively. However, the addition of PVP showed an increase in the maximum peak height (R_{max}) and thus the mean difference between the highest peaks and lowest valley (R_T) increased very much when compared to pristine CA and CPA-0 membrane.

From the obtained data, it was noted that the membrane with the additive exhibited higher roughness value, and this could be due to the firmness of polymer chain packing in the skin layer having large number of pores [24]. Also, the surface roughness of the polymeric asymmetric membrane is directly related to the bond strength of the membrane. Hence, CPA-2 membrane shows increased roughness factor that creates greater adhesive strength and thus leads to better efficacy in the separation process. Moreover, increased surface roughness could retain water molecules for a longer time, which results in increased water permeability, a desirable property of a synthesized CPA-2 membrane for the intended application.

4. Contact Angle Measurements

The measurement of water contact angle at thermodynamic equilibrium was made to determine its wettability and to identify the hydrophobic or hydrophilic property of the prepared membrane surfaces. These properties were employed to examine the antifouling parameter in the developed membranes. In the analysis of contact angle, the interaction between the membrane and liquid is referred as wettability. It depends upon three factors: chemical composition of the membrane surface, porosity and its surface roughness [1]. When the interaction between liquid and membrane is strong, the liquid spreads instantaneously and wets the surface quickly. However, if the interactions are weak, the liquid wets the membrane surface to a certain extent and it also has a vital role in determining the contact angle and surface energy parameters.

In the current study, the parameter of contact angle and surface free energy studies were carried out for the pristine and blend membranes with and without PVP additive. The outcomes are listed in Table 3. The pure CA membrane exhibited a contact angle of 49°, whereas CPA-0 membrane exhibited a contact angle of 57°. Further, it was observed that the contact angle dropped from 57° to 38° with increase in PVP wt% from 0 to 5% and this is because of the surface porosity and the capillary force, which made the water droplet to penetrate slowly into the pores. The contact angle of all the fabricated membranes was less than 90°, indicating the hydrophilic nature of the membrane. The role of each atom and its constituent group in increasing the wettability of the polymeric membrane is in the sequence of N>O>I>Br>Cl>H>F [1]. The increase in hydrophilicity, i.e., the wettability in the CA/PVDF/PVP, could be because of nitrogen that is present, and CPA-0 membrane showed increased contact angle due to the presence of F atom.

The variables like surface free energy (Υ_{sv}), interfacial free energy (Υ_{sl}), work of adhesion (W_a) and spreading coefficient were found by employing the measured contact angle. The surface free energy was found to increase from 52.8 (Pristine) to 59.3 mNm^{-1} (CPA-2) and the interfacial free energy decreased from 5.57 mNm^{-1} to 2.56 mNm^{-1}. This result shows the presence of high hydrophilicity. In membrane application, particularly in bioseparation process, the decreased interfacial free energy is correlated to lower fouling because it weakens the interaction of foulant on the surface of the membrane. The work of adhesion and spreading coefficient of pristine membrane and CPA-2 increased from 118.93 mNm^{-1} to 128.74 mNm^{-1} and −25.06 to −15.26, respectively. Work of adhesion depicts the separation between two adjacent phases of liquid-solid phase boundary from one another and is a measure of the strength of the contact between two phases.

From the above values, it can be concluded that the wetting

Table 3. Contact angle measurements

Membrane	Contact angle (°)	Surface free energy (Υ_{sv}) (mN/m)	Interfacial free energy (Υ_{sl}) (mN/m)	Work of adhesion (W_a) (mN/m)	Spreading coefficient (S_c) (mN/m)
Pristine	49	52.8	5.57	118.93	−25.06
CPA-0	57	48.3	9.08	110.58	−33.42
CPA-1	45	55.5	4.60	122.55	−21.44
CPA-2	38	59.3	2.56	128.74	−15.26

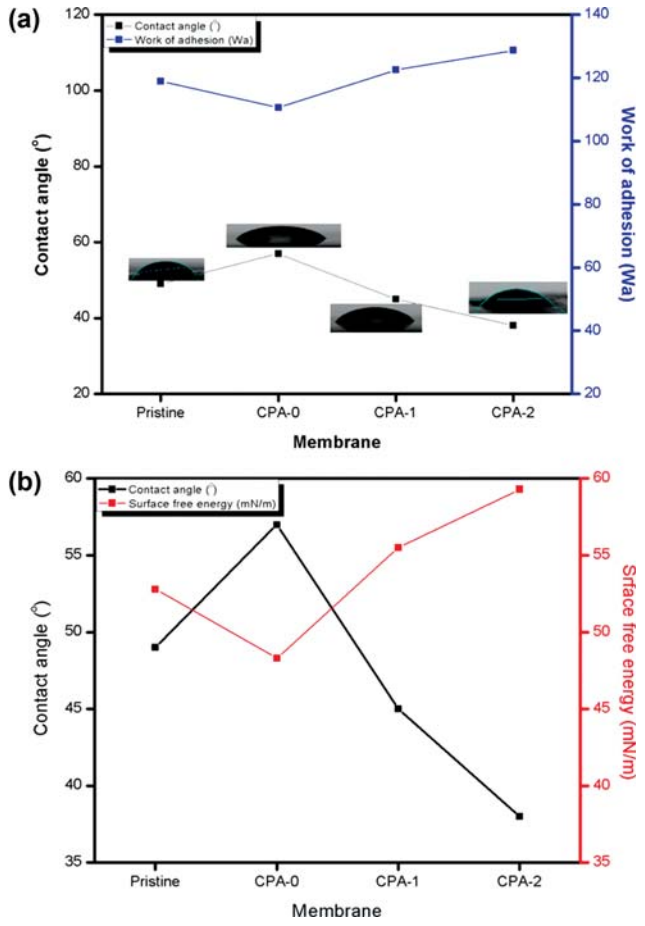

Fig. 5. (a) Contact angle and work of adhesion, and (b) contact angle and surface free energy of the prepared membranes.

property of the blend membrane is increased. Further, as contact angle increases, the work of adhesion and the surface free energy values are found to decrease and these are shown in Fig. 5.

5. Viscosity Measurement of the Casting Solutions

The viscosity of the casting solution depends upon several factors, such as nature of the polymer (concentrations and molecular weight) and that of the solvent, temperature and shear rate. The casting solution would exhibit higher viscosity in a good solvent and the viscosities were directly proportional to molecular weight. During phase inversion process, the rate of exchange between the solvent and non-solvent is influenced by the casting solution and this alters the precipitation kinetics, which has an effect on morphology of the membrane [29]. From Table 4, the result vividly shows an increase in solution viscosity in the presence of PVDF and PVP. The viscosity steadily increases from 191 mPa s (Pristine) to 213 mPa s (CPA-2). Because of higher viscosity, there is a fall in the diffusional rate of exchange among solvent and non-solvent in the process of membrane formation [33]. The higher viscosity also contributes to delayed demixing that leads to the development of thin skin layer and decrease in pore size and macrovoids in the substructure of the membrane, which is clearly shown in Fig. 3 of SEM. Hence, in the membrane preparation, viscosity of casting solution has a vital role in membrane morphology.

Table 4. Equilibrium water content, viscosity, porosity and mean pore radius of the membranes

Membrane	Equilibrium water content (%)	Viscosity (mPa s)	Porosity (%)	Pore radius (nm)
Pristine	64	191	36	29.38
CPA-0	57	198	32	28.92
CPA-1	68	203	45	30.66
CPA-2	75	213	51	32.18

6. Equilibrium Water Content (EWC)

The most effective way to estimate the bulk hydrophilicity of the prepared membrane is by determining its equilibrium water content. EWC mostly depends on two parameters, primarily the existence of quantity of hydrophilic sites with polar functional groups per unit area of membrane medium and another one, the structure of the membrane, i.e., the occurrence of macrovoids in the membrane sub-layers [34]. EWC of the pristine and blend membranes results are listed in Table 4. The blend membrane CPA-0 showed slight decrement in water content (57%) when compared to pristine (64%). This is due to the presence of fluoride group in the PVDF shown in FTIR spectra of Fig. 2 (CPA-0) and has fewer hydrophilic sites and macrovoids as shown in Fig. 3(b). This plays a vital role in reduction of water content. However, the results in Table 4 reveal that there is an increase in water content for CPA-1 and CPA-2 showing rise in hydrophilicity of the membrane with additive, when compared to pristine and CPA-0. The increase in hydrophilicity improves the affinity of the blend membrane matrix towards the water molecule, resulting in higher water content of CPA-2 membrane, as clearly depicted in SEM image of Fig. 3(d).

7. Porosity and Mean Pore Size of the Prepared Membranes

The rejection and intrinsic permeation property of the membrane depends upon the overall pore size and pore size distribution, i.e., porosity of the membrane. Table 4 presents the effect of hydrophilic additive on membrane porosity. Pristine membrane porosity was found to be 36% and the addition of PVDF exhibited a decrease in porosity of 32%. This decrease in porosity is because of the formation of dense parts, which decreased the macrovoids, resulting in lesser porosity. The reduction in macrovoids was also noticed from the cross sectional image of SEM. The modified membrane with PVP additive resulted in increase in porosity from 45% to 51% and pore radius from 28.32 to 32.18 nm when the percentage of PVP increased from 2.5% to 5%. The rise in membrane porosity was a result of rise in viscosity of dope solution which delayed the rate of exchange within the solvent and non-solvent in the precipitation bath. Further, a dense top layer was formed in the membrane with higher porosity, which was due to delayed demixing. Also, leaching out of PVP from the casting film could be another reason for the enhancement of pores.

8. Mechanical Property of the Membrane

Mechanical properties are expressed in terms of strength, stiffness and toughness of the membrane to determine its overall mechanical stability. When a mechanical load is applied to asymmetric membrane, its response may be either the change in shape and dimensions or fracture. When load is applied, the magnitude effect of the membrane depends on the specific type of intermo-

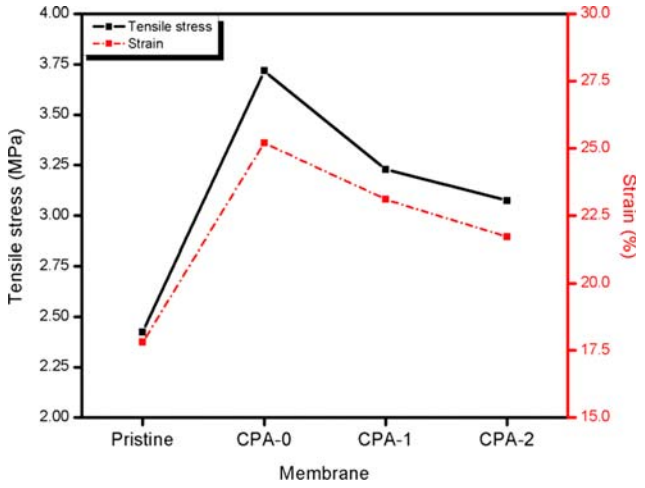

Fig. 6. Mechanical properties of prepared membranes.

lecular bonding and also on the main chain chemical group of overall chain flexibility. Fig. 6 displays the mechanical properties of the pristine as well as blend membranes by carrying out tensile test and is described by stress-strain curve. The tensile stress and strain of pristine membrane were found to be 2.424 MPa and 17.8%, respectively. On addition of PVDF, both tensile stress and strain showed an increased value of 3.718 MPa and 25.2%, respectively. This increase could be due to the strong interfacial adhesion, better interaction and good dispersion between polymeric chains. On the other hand, CA/PVDF blend membrane with PVP as an additive possessed tensile stress and strain of 3.228 MPa and 23.1% for CPA-1 and 3.074 MPa and 21.7% for CPA-2, respectively. The slight decrease in mechanical properties might be due to the development of more pores, pore size distribution (Fig. 3(d)) and increase in porosity values as shown in Table 4. Based on the results, it was evident that the mechanical properties of the blend membrane with additive improved when compared to pristine membrane.

Table 5. Thermal gravimetric analysis parameters for the prepared membranes

Parameter	Membranes			
	Pristine	CPA-0	CPA-1	CPA-2
IDT (°C)	94.36	162.69	185.84	204.02
T_d (°C)	217.68	318.49	338.23	352.63

9. Thermal Property of the Membrane

Thermogravimetric analysis gives information on weight loss with temperature, which helps in determining the thermal stability of the polymeric membrane. It also provides the amount of moisture and volatile matter present in the prepared membrane.The thermal analysis results of the pristine membrane and CA/PVDF membranes with and without additive are presented in Fig. 7. Thermal stability parameters--IDT (intial decomposition temperature) and T_d (thermal degradation) estimated at 5% wt loss from TGA--are tabulated in Table 5. It was clearly observed that on thermal treatment, pristine membrane undergoes intial decomposition at 94 °C and thermal degradation at 217.68 °C. However, the prepared blend membranes with and without additive showed higher IDT and T_d when compared to pristine membrane. When the concentration of PVP increased, the IDT increased fom 162.69 °C to 204.02 °C and T_d increased from 318.49 °C to 352.63 °C. These results prove that membranes with PVP additive show more thermal stability.

10. Pure Water Flux (PWF)

Ultrafiltration experimental tests were conducted to evaluate the permeability and antifouling property of the membranes. PWF depends upon various factors, such as water content, membrane porosity, structural morphology and topography of membrane and contact angle, i.e., hydrophilicity of membrane. After compaction of the membranes, pure water flux was measured at the TMP of 0.3 MPa. The pure water flux of the fabricated membranes is illustrated in Fig. 8. The lower PWF of 141.7 L m^{-2} h^{-1} observed for pristine

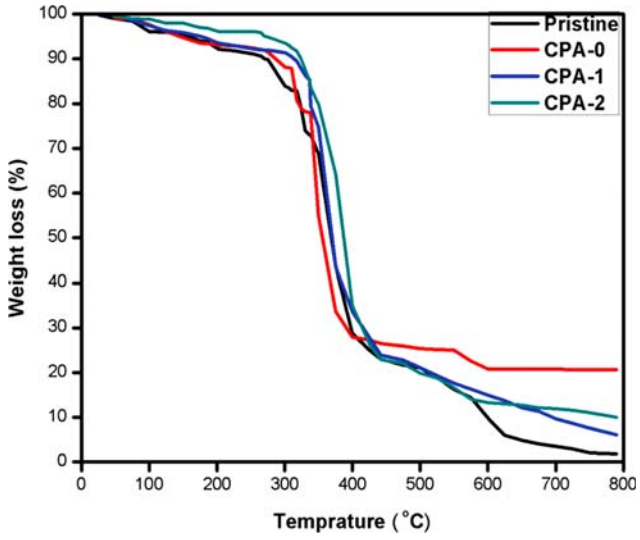

Fig. 7. Thermal gravimetric analysis of the membranes.

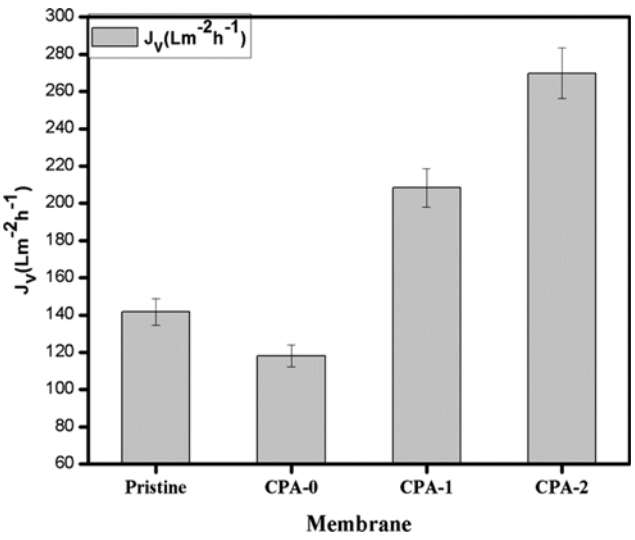

Fig. 8. PWF values of the membranes at 0.3 MPa TMP.

membrane was due to the repulsion among the bulky acetate groups, which significantly lowered the competency and demolition of the water molecules. In CPA-0 membrane, PWF showed the lowest flux value of 118.6 L m^{-2} h^{-1}. This decrease in PWF is due to the formation of extremely firm polymer matrix, which reduces the pores over the top surface layer of the membrane as shown in Fig. 3(b) and hence decrease in porosity as given in Table 4. Further, the addition of PVDF to pristine membrane led to a rise in contact angle as shown in Table 3 and hence resulted in lesser hydrophilicity. The PWF of the CPA-1 and CPA-2 membrane showed higher flux values compared to pristine and CPA-0 membrane. When PVP concentration increased from 2.5 wt% to 5 wt%, the PWF increased from 208.32 L m^{-2} h^{-1} to 269.82 L m^{-2} h^{-1}. The considerable change in the PWF rate of CPA-1 and CPA-2 is due to the leachability of water-soluble additive during gelation process. This gave rise to the development of larger pores in the membranes, which increased porosity (Table 4), and is also evident from SEM images of Fig. 3(c) and 3(d). It is observed that PVP added membrane is more hydrophilic when compared to pristine and CPA-0. Therefore, as the concentration of PVP increased, the contact angle decreased, resulting in higher membrane hydrophilicity, so it exhibited enhanced water permeation. Hence these aspects created a remarkable increase in the PWF.

11. Antifouling Studies on BSA and SA

In membrane technology, fouling is a serious issue that limits the extended utilization of the membranes. The adsorption or deposition of the rejected particles on the surface of membrane or inside the membrane pores leads to fouling. Membrane fouling may be classified as hydraulic reversible or irreversible fouling. In hydraulically reversible fouling, the attachment of foulants on the surafce is very weak and freely linked to the membrane. So it can be easily detached by physical cleaning or backwashing using deionized or demineralized water. In irreversible fouling, the physical cleaning is not possible to remove the foulants because the fouling agents are strongly adsorbed or deposited inside the membrane pores and so it can be removed only by chemical cleaning.

The antifouling properties of the pristine membrane and CA/PVDF blend membrane with and without PVP additive were analyzed by determining the PWF of cleaned membrane fouled by carrying out the filtration experiments with 1 g/L of BSA and SA solution. The PWF (J_{v1}), BSA and SA flux (J_p and J_s) and PWF after cleaning the membrane (J_{v2}) are presented in Figs. 9 and 10. It is evident from Fig. 9 and 10 that the values of J_{v1}, J_p, J_s and J_{v2} decreased with increase in time for all the synthesized membrane. Fig. 11 and 12 illustrate the FRR and antifouling properties against BSA and SA. From the obtained results, CPA-2 membrane showed better FRR of 94.3% when compared to prsitine, exhibiting 77.65% against BSA. The BSA flux values for CPA-0 blend membrane exhibited lowest values of J_p - 56.37 L m^{-2} h^{-1} and J_{v2} - 77.78 L m^{-2} h^{-1} (Table 6) and this is due to the lesser hydrophilic nature of the membrane

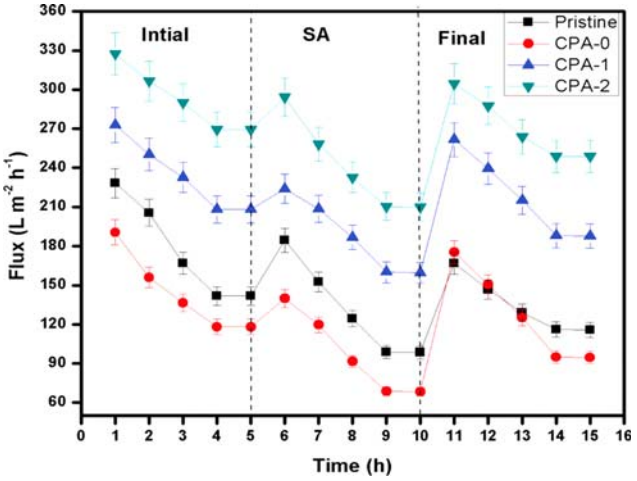

Fig. 10. Flux variations of the membranes at a transmembrane pressure of 0.3 MPa for Pristine, CPA-0, CPA-1 and CPA-2 membranes. (1) Initial PWF (0-5) h. (2) SA flux rate (5-10) h. (3) PWF of cleaned membranes (10-15) h.

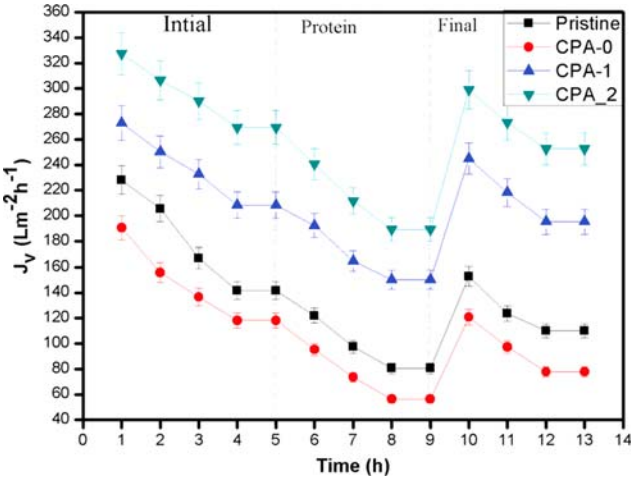

Fig. 9. Flux variations of the membranes at a transmembrane pressure of 0.3 MPa for Pristine, CPA-0, CPA-1 and CPA-2 membranes. (1) Initial PWF (0-5) h. (2) BSA protein flux rate (5-9) h. (3) PWF of cleaned membranes (9-13) h.

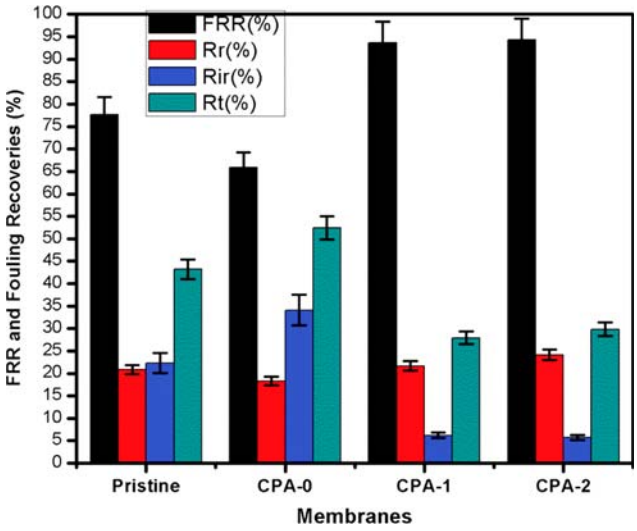

Fig. 11. FRR and antifouling properties against BSA on Pristine, CPA-0, CPA-1 and CPA-2 membrane.

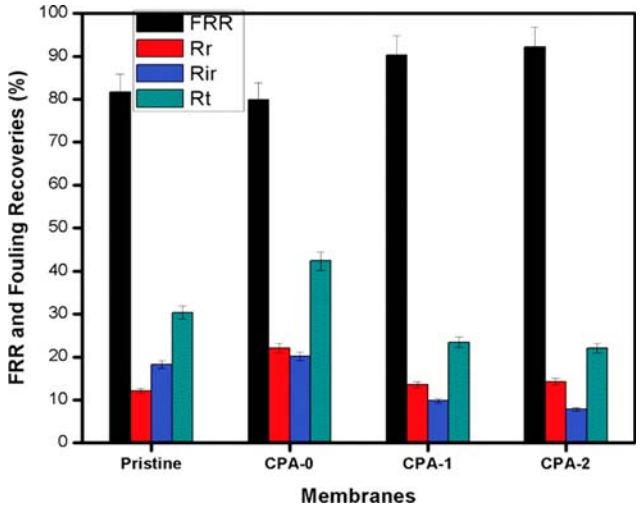

Fig. 12. FRR and antifouling properties againt SA on Pristine, CPA-0, CPA-1 and CPA-2 membrane.

as shown in Fig. 5 when compared to other membranes. Though the flux values of CPA-0 blend membrane are less when compared to other prepared membranes, the main objective of adding PVDF to CA is to increase thermal and mechanical properties of the membrane. In antifouling study using BSA, the flux values of J_{v1}, J_p and J_{v2} for CPA-1 were 208.32, 150.14 and 195.35 L m^{-2} h^{-1} and CPA-2 were 269.82, 189.32 and 254.45 L m^{-2} h^{-1}, respectively. The enhanced antifouling properties of CPA-2 membrane are due to the increase in hydrophilicity, hence the water molecules are firmly bound and hinder the binding of BSA molecules to the surface of membrane. Further, the BSA molecules isoeletric point is 4.9 and it exhibits a negative charge in neutral solution [32]. As a result, the surface of the membrane is also negatively charged, so there is a strong electrostatic force of repulsion between BSA and membrane surface reducing fouling for CPA-2 membrane. Similarly, in permeation study using SA solution, the PVP incorporated membranes show enhanced antifouling with better flux recovery ratio. The FRR values of Prsitine, CPA-0, CPA-1 and CPA-2 are 81.7%, 79.82%, 90.3% and 92.18%, respectively. The PWF, permeate flux against SA and flux of cleaned membrane for CPA-2 were found to be 269.82 L m^{-2} h^{-1}, 210.13 L m^{-2} h^{-1} and 248.72 L m^{-2} h^{-1}, whose values are higher when compared to other membranes. The increase in flux values is due to the fact that the pores which are blocked by SA were easily removed by physical cleaning because of the formation of narrow finger-like pore structure discussed earlier in membrane morphology.

From the obtained results, the CPA-2 membrane showed a maximum FRR against BSA and SA than other membranes. This effective increase in FRR values is due to the presence of PVP, which imrpoved the hydrophilicity on the membrane surface. This surface modification promotes negative charged surface and also weakens the attachment of foulant (i.e., BSA and SA) on the membrane surface and it helps in reducing the fouling [12]. Hence, the higher values of FRR of CPA-2 membrane indicate enhanced antifouling properties of the membrane as shown in Fig. 11 and 12.

The hydraulic reversible fouling (R_r), hydraulic irreversible fouling (R_{ir}) and total fouling (R_t) calculated from the J_{v1}, J_p and J_s and J_{v2} of cleaned membranes are shown in Figs. 11 and 12. From the results, the hydraulic reversible ratio of the prepared membranes against BSA is 20.85% (pristine), 18.32% (CPA-0), 21.7% (CPA-1) and 24.14% (CPA-2) and for SA, it is 12.12% (pristine), 22.12% (CPA-0), 13.6% (CPA-1) and 14.3% (CPA-2), respectively. Further, the fouling recoveries of R_r values are greater than the R_{ir} values and it shows that the CPA-1 and CPA-2 membranes are almost reversible. This indicates easy cleaning of the membranes and the membranes could be utilized for greater number of cycles. Therefore, the results clearly demonstrate that the CPA-2 membrane shows greater efficiency in the FRR, reversible fouling and the decrement in the irreversible fouling. Also, the CPA-2 membrane shows significant change in PWF, hydrophilicity and antifouling studies when compared to other membranes.

12. Rejection Studies of BSA and SA

The developed membranes in the current work were used for the elimination of BSA and SA by carrying filtration experiments at TMP of 0.3 MPa and are shown in Fig. 13. The flux decline is the consequence of accumulation of rejected BSA and SA over the membrane surface and pore plugging that hinders the passage of water molecules through the pores of the membrane. From Table 6, the permeation flux J_s and J_p is in the order of CPA-2>CPA-1>Pristine> CPA-0. On comparing the percentage rejection of BSA and SA, CPA-0 showed higher rejection of 86% and 88%, respectively. The percentage rejection of BSA and SA for CPA-1 is 88% and 85% and CPA-2 is 86% and 83%, respectively, which is less when compared to CPA-0 and this could be due to the increase in pore radius (Table 4) of CPA-1 and CPA-2 membranes. The rejection results have good correlation with the flux permeation results and antifouling studies of the membrane. The higher concentration of PVP is responsible for increase in size and distribution of pores that led to increased PWF with slight decrease in BSA and SA rejection. For this reason, it is necessary to develop a membrane not only for

Table 6. Initial water flux (J_{v1}), BSA flux (J_p) and SA flux (J_s) and final water flux (J_{v2}) of the membranes

Membrane code	Pure water flux (L m^{-2} h^{-1}) J_{V1}	Permeate flux (L m^{-2} h^{-1})			
		BSA		SA	
		J_p	J_{v2}	J_s	J_{v2}
Pristine	141.7	80.49	110.04	98.58	115.76
CPA-0	118.6	56.37	77.78	68.43	94.66
CPA-1	208.32	150.14	195.35	159.48	187.32
CPA-2	269.82	189.32	254.45	210.13	248.73

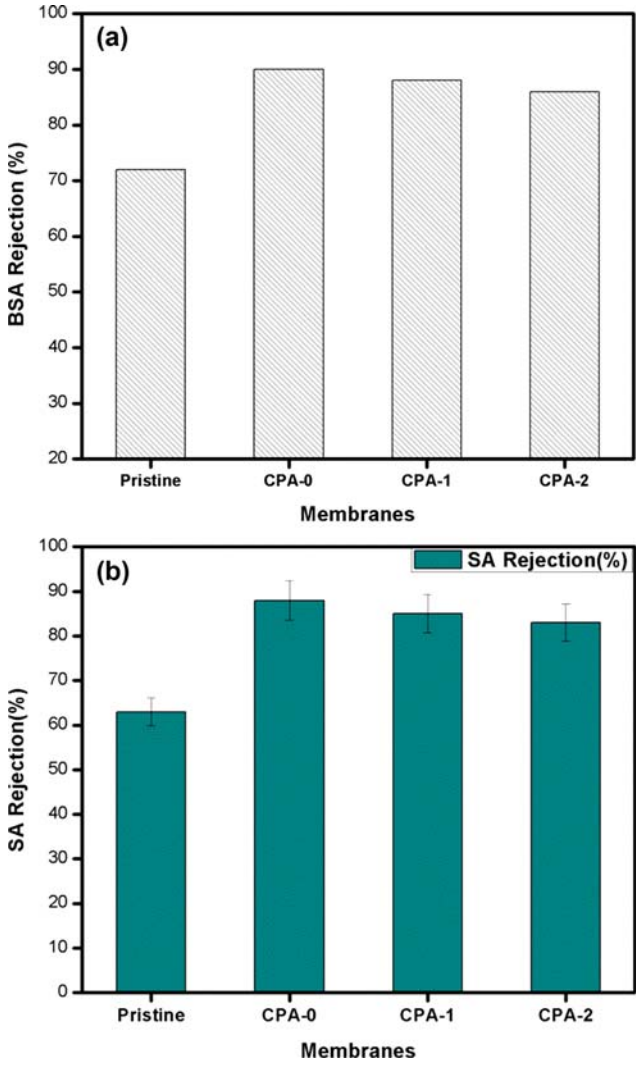

Fig. 13. (a) BSA and (b) SA rejection of the prepared membranes.

rejecton but also with improved hydrophilicity, thermal stability, mechanical stability and the other surface parameters to increase the flux. The acquired results demonstrated that the developed CPA-2 membrane possesses the ability for the rejection of BSA and SA.

Table 7 gives a comparison of PWF, permeation flux, FRR and percentage rejection of BSA and SA for various membranes taken from the literature. From the table, it can be concluded that the synthesized CA/PVDF/PVP membrane showed better performance with good results and it can also be utilized effectively for the rejection of similar molecules as that of BSA and SA.

CONCLUSION

Hydrophilic and hydrophobic polymeric blend membranes were synthesized through phase inversion technique employing PVP additive which acts as a pore forming agent. A detailed study was carried out by comparing the performance of membranes with and without additive. The effect of PVP concentration on the membrane properties, such as morphology, permeation, porosity and hydrophilicity, was assesed. FTIR-ATR results showed the existence of the same functional groups in all the prepared membranes except for the difference in the intensity of the peaks. SEM analysis of the blend membrane revealed that with increase in concentration of PVP, defect-free skin layer and substructure with macrovoids were formed. Also, the pores were narrow, uniform and well developed. AFM analysis exhibited that the topograpghy and roughness of the membranes were enhanced by the incorporation of PVP to the CA/PVDF blend solution. Surface energy parameters determined using contact angle data revealed that the interfacial free energy of the blend membranes was less compared to the pristine membrane. The results of contact angle, EWC and porosity showed a considerable increase in hydrophilicity of the blend membranes with the incorporation of PVP. Further, there was a substantial increase in the porosity and mean pore radius values due to delayed demixing during membrane formation. From the obtained results, PVP

Table 7. Comparison of PWF, permeation, FRR, % rejection of various membranes

Membrane	PWF ($L\ m^{-2}\ h^{-1}$)	Permeation flux ($L\ m^{-2}\ h^{-1}$)		FRR (%)		Rejection (%)		Reference
		BSA	SA	BSA	SA	BSA	SA	
CA/PSF/PEG	115	74.5	-	-	-	69.6		[2]
CAB hollow fiber membrane	188	-	-	-	-	-	75	[4]
PVDF/CA	522	285		78.2	-	-		[11]
CA/CMCA	73.2	68		78.2	-	86.3		[12]
PSF/PBI	355	-		93.5	-	68.66		[16]
CA/PVP/TiO_2	416	-		91.1	-	94.3		[18]
PES/ SiO_2	87.2	-		85	-	93.6		[19]
CA/PEG	130.7	21.5		91	-	96.9		[21]
CA/PVP	150.7	17.2		54	-	77.9		[21]
PMIA/LiCl/PEG	276.3	50		91	-	81		[23]
PEI/citric acid	242.3	14.2	-	76	-	-		[29]
PSF/ TiO_2	61	-		68	-	93		[35]
PSF/$CaCO_3$	60	-		51	-	90		[36]
CA/PVDF/PVP	269.82	189.32	210.13	94.3	92.18	86	83	Present study

incorporated membranes had better thermal stability but with slight decrease in mechanical stability. In the performance studies, the permeation results indicated an improvement in PWF of 269.82 L m^{-2} h^{-1} with flux recovery ratio of up to 94.3% (BSA) and 92.18% (SA) for the CPA-2 membrane. In the rejection studies, CPA-2 membrane showed slightly decreased rejection of BSA (83%) and SA (86%), and this is because of increase in concentration of PVP which forms more number of pores on the surface of membrane. However, the performance studies revealed that the CPA-2 membrane offered increased pure water flux, permeability, optimal rejection and antifouling properties when compared to CPA-1, CPA-0 and pristine membranes. Moreover, the CPA-2 membrane also had better results in surface morphology, surface roughness and hydrophilicity than other membranes. Thus, it is concluded that the synthesized CPA-2 membrane is appropriate for the rejection and recovery of protein (BSA) and polysaccharide (sodium alginate). The overall results indicate that the synthesized CPA-2 membrane can be further utilized for commercial purpose, especially in bioseparation application.

NOMENCLATURE

A : area of the membrane [cm^2]
BSA : bovine serum albumin
CA : cellulose acetate
C_f : concentration of the feed [gL^{-1}]
C_p : concentration of the permeate [gL^{-1}]
CPA-0 : CA/PVDF without PVP (0 wt%)
CPA-1 : CA/PVDF with PVP (2.5 wt%)
CPA-2 : CA/PVDF with PVP (5 wt%)
DMF : dimethyl formamide
EWC : equilibrium water content
FRR : flux recovery ratio
IDT : intial decomposition temperature [°C]
J_p : protein permeate flux [L m^{-2} h^{-1}]
J_s : sodium alginate permeate flux [L m^{-2} h^{-1}]
J_{v1} : initial pure water flux [L m^{-2} h^{-1}]
J_{v2} : final pure water flux [L m^{-2} h^{-1}]
L : thickness of the membrane [cm]
PB : phosphate buffer
PVDF : poly(vinylidene fluoride)
PVP : polyvinylpyrrolidone
PWF : pure water flux
Q : volume of the permeate per unit time [m^3s^{-1}]
R_a : mean roughness profile [nm]
R_{ir} : irreversible protein fouling
r_m : average pore size [nm]
R_{max} : maximum height of the roughness profile [nm]
R_q : root mean square deviation roughness [nm]
R_r : reversible protein fouling
R_t : total protein fouling
R_T : total height of the roughness profile [nm]
SA : sodium alginate
S_c : spreading coefficient [mNm^{-1}]
T_d : thermal degradation at 5% wt loss [°C]
TMP : trans membrane pressure [MPa]
W_a : work of adhesion [mNm^{-1}]
WCA : water contact angle
W_d : weight of the dry sample [g]
W_w : weight of the wet sample [g]

Greek Letters

β : constant value of 0.0001024 mJm^{-2}
ε : porosity of the membrane
η : water viscosity [Pa s]
θ : solid-liquid contact angle
ρ : density of pure water [g cm^{-3}]
Υ_{lv} : interfacial free energies of liquid-vapor [mNm^{-1}]
Υ_{sl} : interfacial free energies of solid-liquid [mNm^{-1}]
Υ_{sv} : interfacial free energies of solid-vapor [mNm^{-1}]
ΔP : trans-membrane pressure [Pa]
Δt : time duration of permeate [h]

REFERENCES

1. S. Rajesh, K. H. Shobana, S. Anitharaj and D. R. Mohan, *Ind. Eng. Chem. Res.*, **50**, 5550 (2011).
2. M. Sivakumar, D. R. Mohan and R. Rangarajan, *J. Membr. Sci.*, **268**, 208 (2006).
3. A. W. Zularisam, A. F. Ismail, M. R. Salim, M. Sakinaha and H. Ozaki, *Desalination*, **212**, 191 (2007).
4. M. Hashino, T. Katagiri, N. Kubota, Y. Ohmukai, T. Maruyama and H. Matsuyama, *J. Membr. Sci.*, **366**, 258 (2011).
5. G. F. Crozes, J. G. Jacangelo, C. Anselme and J. M. Laine, *J. Membr. Sci.*, **124**, 63 (1997).
6. W. Yuan and A. L. Zydney, *Environ. Sci. Technol.*, **34**, 5043 (2000).
7. M. Liu, C. Xiao and X. Hu, *Desalination*, **298**, 59 (2012).
8. D.-Q. Cao, X.-D. Hao, Z. Wang, X. Song, E. Iritani and N. Katagiri, *J. Membr. Sci.*, **535**, 312 (2017).
9. K. Katsoufidou, S. G. Yiantsios and A. J. Karabelas, *J. Membr. Sci.*, **300**, 137 (2007).
10. K. Kimura, Y. Hane, Y. Watanabe, G. Amy and N. Ohkuma, *Water Res.*, **38**, 3431 (2004).
11. M. H. Razzaghi, A. Safekordi, M. Tavakolmoghadam, F. Rekabdar and M. Hemmati, *J. Membr. Sci.*, **470**, 547 (2014).
12. B. Han, D. Zhang, Z. Shao, L. Kong and S. Lv, *Desalination*, **311**, 80 (2013).
13. H. Kamal, F. M. Abd-Elrahim and S. Lofty, *J. Radiat. Res. Appl. Sci.*, **7**, 146 (2014).
14. S. Vidya and D. Mohan, *Sep. Sci. Technol.*, **45**, 740 (2010).
15. Y. Ertas and T. Uyar, *Crabohyd. Polym.*, **177**, 378 (2017).
16. M. K. Irfana, Arun M. Isloor, A. F. Ismail, O. Abdulrahman and H. K. Fun, *Desalin. Water Treat.*, **57**, 19810 (2015).
17. L.-F. Fang, H.-Y. Yang, L. Cheng, N. Kato, S. Jeon, R. Takagi and H. Matsuyama, *Ind. Eng. Chem. Res.*, **56**, 11302 (2017).
18. E. Eren, A. Sarihan, B. Eren, H. Gumus and F. O. Kocak, *J. Membr. Sci.*, **475**, 1 (2015).
19. F. S. Dehkordi, M. Pakizeh and M. Namvar-Mahboub, *Appl. Clay Sci.*, **105**, 178 (2015).
20. K. A. Gebru and C. Das, *J. Environ. Manage.*, **200**, 283 (2017).
21. M. S. Muhamad, M. R. Salim and W.-J. Lau, *Korean J. Chem. Eng.*, **32**, 2319 (2015).

22. S. Abdolhamid, M. Toraj, R. M. Behbahani and M. Hemati, *Adv. Polym. Technol.*, **34**, 21494 (2015).
23. K. A. Gebru and C. Das, *Chin. J. Chem. Eng.*, **25**, 911 (2017).
24. J. S. Beril Melbiah, D. Nithya and D. Mohan, *Colloids Surf. A Physicochem. Eng. Asp.*, **516**, 147 (2017).
25. Pramila, J. S. Beril Melbiah, D. Rana, N. Nagendra Gandhi, A. Nagendran and D. Mohan, *Polym. Test.*, **67**, 218 (2018).
26. D. Y. Kwok and A. W. Neumann, *Colloids Surf. A: Physicochem. Eng. Asp.*, **161**, 31 (2000).
27. S. Zha, J. Yu, G. Zhang, N. Liu and R. Lee, *RSC Adv.*, **5**, 105692 (2015).
28. M. Safarpour, V. Vatanpour and A. Khataee, *Desalination*, **393**, 65 (2016).
29. R. S. Hebbar, A. M. Isloor, A. F. Ismail, S. J. Shilton, O. Abdulrahman and H. K. Fun, *New J. Chem.*, **39**, 6141 (2015).
30. P. Maheswari, P. Barghava and D. Mohan, *J. Polym. Res.*, **20**, 1 (2013).
31. J. Dasgupta, S. Chakraborty, J. Sikder, R. Kumar, D. Pal, S. Curcio and E. Drioli, *Sep. Purif. Technol.*, **133**, 55 (2013).
32. M. Kumar and J. Lawler, *Sep. Purif. Technol.*, **130**, 112 (2014).
33. W.-Z. Lang, L.-F. Chu and Y.-J. Guo, *J. Appl. Polym. Sci.*, **121**, 1961 (2011).
34. R. S. Hebbar, A. M. Isloor, B. Prabhu, Inamuddin, A. M. Asiri and A. F. Ismail, *Sci. Rep.*, **8**, 4665 (2018).
35. G. Zhang, L. Zhang, S. Lu, Q. Meng, C. Shen and J. Zhang, *J. Membr. Sci.*, **436**, 163 (2013).
36. A. K. Nair, A. M. Isloor, R. Kumar and A. F. Ismail, *Desalination*, **322**, 69 (2013).